

# Angular magnetoresistance oscillations in quasi-one-dimensional organic conductors in the presence of a crystal superstructure

Anand Banerjee and Victor M. Yakovenko

Joint Quantum Institute and Center for Nanophysics and Advanced Materials,  
Department of Physics, University of Maryland, College Park, Maryland 20742-4111, USA  
(Dated: **cond-mat/0608317, v.1 August 14, 2006, v.2 July 8, 2008**)

We study the effect of crystal superstructures, produced by orientational ordering of the  $\text{ReO}_4$  and  $\text{ClO}_4$  anions in the quasi-one-dimensional organic conductors  $(\text{TMTSF})_2\text{ReO}_4$  and  $(\text{TMTSF})_2\text{ClO}_4$ , on the angular magnetoresistance oscillations (AMRO) observed in these materials. Folding of the Brillouin zone due to anion ordering generates effective tunneling amplitudes between distant chains. These amplitudes cause multiple peaks in interlayer conductivity for the magnetic field orientations along the rational crystallographic directions (the Lebed magic angles). Different wave vectors of the anion ordering in  $(\text{TMTSF})_2\text{ReO}_4$  and  $(\text{TMTSF})_2\text{ClO}_4$  result in the odd and even Lebed angles, as observed experimentally. When a strong magnetic field is applied parallel to the layers and perpendicular the chains and exceeds a certain threshold, the interlayer tunneling between different branches of the folded electron spectrum becomes possible, and interlayer conductivity should increase sharply. This effect can be utilized to probe the anion ordering gaps in  $(\text{TMTSF})_2\text{ClO}_4$  and  $(\text{TMTSF})_2\text{ReO}_4$ . An application of this effect to  $\kappa\text{-(ET)}_2\text{Cu(NCS)}_2$  is also briefly discussed.

PACS numbers: 74.70.Kn, 72.15.Gd, 73.21.Ac

## I. INTRODUCTION

The quasi-one-dimensional (Q1D) organic conductors  $(\text{TMTSF})_2\text{X}$  (where TMTSF is tetramethyltetraselenafulvalene, and X represents a monovalent anion, such as  $\text{PF}_6$ ,  $\text{ClO}_4$ , or  $\text{ReO}_4$ ) have very interesting physical properties, including the quantum Hall effect and possibly triplet superconductivity [1, 2]. These materials consist of parallel conducting chains along the  $x$  axis, arranged in layers with the interchain spacing  $b$  along the  $y$  axis and the interlayer spacing  $c$  along the  $z$  axis. The electron tunneling amplitudes between the TMTSF molecular sites are highly anisotropic in the three directions:  $t_a : t_b : t_c = 2500 : 250 : 10$  K [1].

These materials exhibit the angular magnetoresistance oscillations (AMRO), where resistivity strongly changes as a function of the magnetic field orientation. There are three basic types of AMRO: the Lebed magic angles [3, 4, 5, 6, 7] for the magnetic field rotation in the  $(y, z)$  plane, the Danner-Kang-Chaikin (DKC) oscillations in the  $(x, z)$  plane [8, 9], and the third angular effect in the  $(x, y)$  plane [10, 11, 12]. The Lebed oscillations manifest themselves as sharp peaks in the interlayer conductivity  $\sigma_{zz}$  occurring when the magnetic field points from one chain to another along a rational crystallographic direction, as illustrated in Fig. 1. Approximating the triclinic crystal lattice of  $(\text{TMTSF})_2\text{X}$  by the orthogonal one, the magic Lebed angles can be written as

$$\frac{B_y}{B_z} \frac{c}{b} = \frac{n}{m} \Leftrightarrow \sin \varphi \tan \theta = \frac{n}{m} \frac{b}{c}, \quad (1)$$

where  $n$  and  $m$  are integer numbers, and  $\mathbf{B} = (B_x, B_y, B_z) = B(\sin \theta \cos \varphi, \sin \theta \sin \varphi, \cos \theta)$  is the magnetic field. Experimentally, the Lebed effect is the most pronounced for  $m = 1$ . Lee and Naughton [13, 14] studied AMRO for generic orientations of  $\mathbf{B}$ , where all three

effects coexist. They found that the Lebed oscillations are enhanced when  $B_x \neq 0$  [13], and the DKC oscillations still exist in the presence of  $B_y \neq 0$  [14].

Although initially the different types of AMRO were treated as separate phenomena, a unified picture emerged in the recent years due to substantial experimental and theoretical progress. A three-dimensional visualization of the experimentally measured  $\sigma_{zz}(\mathbf{B})$  [15] demonstrated that the different types of AMRO can be viewed as modulations of the basic Lebed resonances. Measurements with carefully placed electric contacts [16] proved that AMRO exist only in the transverse resistance  $R_{zz}$  and not in the longitudinal resistance  $R_{xx}$  along the chains. Theory always predicted this difference, but many experiments observed AMRO in  $R_{xx}$  as well because of mixing between different components of the conductivity ten-

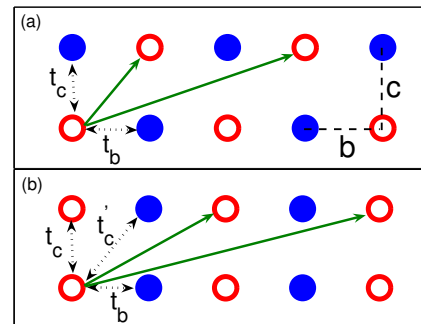


FIG. 1: A view along the chains of a Q1D metal with the anion ordering at a wave vector  $\mathbf{Q}$ . The filled and open circles represent the chains with the energies  $\pm E_g$ . (a)  $(\text{TMTSF})_2\text{ReO}_4$ ,  $\mathbf{Q} = (0, 1/2, 1/2)$ . (b)  $(\text{TMTSF})_2\text{ClO}_4$ ,  $\mathbf{Q} = (0, 1/2, 0)$ .

sor. AMRO were found not only in the dc conductivity, but also in the ac conductivity at microwave frequencies [17, 18]. The ac measurements were interpreted in terms of the so-called period orbit resonance (POR) [19], which is a generalization of the cyclotron resonance to more complicated (e.g., open) Fermi surfaces [20]. The ac resonances occur at the angles depending on frequency  $\omega$  and deviating from Eq. (1) [17, 18], so the Lebed magic angles are not truly magic [21, 22]. This observation eliminates theoretical scenarios proposing a radical change in the ground state of the system depending on the magnetic field orientation along the magic or non-magic angles. This conclusion is also supported by the absence of any angular effect in NMR [23].

Given these experimental facts, AMRO most likely represent some sort of a resonance effect in the dc and ac transport coefficients. The first theoretical calculation along these lines was done in Ref. [24] using the Kubo formula with the electron wave functions for a magnetic field in the  $(y, z)$  plane. This quantum-mechanical calculation was then generalized to include the  $B_x$  component of the magnetic field [25] and the anion superstructure of  $(\text{TMTSF})_2\text{ClO}_4$  [26, 27]. In another theoretical approach, the Boltzmann kinetic equation was solved for a constant relaxation time  $\tau$  by using quasiclassical electron trajectories on the Fermi surface [11, 12, 13, 14, 19, 20, 28, 29, 30, 31]. This solution can be written in a general form using the so-called Shockley tube integral [32] or the Chambers formula [33], see also the book [34]. In the third theoretical approach, the interlayer conductivity was calculated using a perturbation theory in the electron tunneling amplitude between two layers [35, 36, 37]. In this approach, AMRO originate from the Aharonov-Bohm quantum interference in interlayer tunneling in the presence of a magnetic field [37]. All these three seemingly different theoretical approaches produce the same final results and are essentially equivalent.

Interestingly, the model of a Q1D bilayer in a magnetic field [37] is mathematically equivalent to a superconducting qubit driven by an ac electric field and detuned by a dc field [38, 39, 40, 41, 42]. The Mach-Zehnder interference pattern found for the superconducting qubit (the so-called Bessel staircase) [38, 39] is essentially the same as the AMRO pattern in Q1D conductors derived from the Aharonov-Bohm quantum interference [37]. The same equations also describe laser cooling of trapped ions [43]. The similarity in the behavior of these systems demonstrates that quantum coherence in the Q1D organic conductors at low temperatures is as high as in the superconducting qubits and ion traps, which are actively considered for applications in quantum computing and quantum information.

Despite substantial progress in understanding of AMRO in Q1D conductors, some experimental results remain unexplained. One open problem is the angular oscillations of the Nernst effect [44]. Another unresolved problem is the angular minimum and saturation of the

interlayer resistivity  $R_{zz}$  observed for a magnetic field in the  $y$  direction [6, 14, 15, 45]. Although the manifestations of AMRO are qualitatively similar in all members of the  $(\text{TMTSF})_2\text{X}$  family, direct comparison of the measurements in  $(\text{TMTSF})_2\text{PF}_6$ ,  $(\text{TMTSF})_2\text{ClO}_4$ , and  $(\text{TMTSF})_2\text{ReO}_4$  shows substantial differences [45].

For a magnetic field rotation in the  $(y, z)$  plane with  $B_x = 0$ , only three strong Lebed peaks in  $\sigma_{zz}$  with  $n = 0, \pm 1$  are observed in  $(\text{TMTSF})_2\text{PF}_6$  [6, 45]. When special care is taken to ensure that  $B_x = 0$ , the very weak peaks with  $n = \pm 2$  in  $(\text{TMTSF})_2\text{PF}_6$  disappear completely [15]. In contrast, in  $(\text{TMTSF})_2\text{ReO}_4$ , strong Lebed oscillations are observed up to  $n = \pm 11$  [46]. In  $(\text{TMTSF})_2\text{ClO}_4$ , the Lebed oscillations are much weaker in amplitude than in  $(\text{TMTSF})_2\text{PF}_6$  and  $(\text{TMTSF})_2\text{ReO}_4$  [45], but many Lebed resonance can be detected after differentiation of the data with respect to the angle of rotation [4, 5]. The strength of the DKC oscillations is also very different in these materials. The DKC oscillations are quite strong in  $(\text{TMTSF})_2\text{ClO}_4$ , where they were originally discovered [8]. In  $(\text{TMTSF})_2\text{PF}_6$ , Ref. [9] found very weak DKC oscillations, but Ref. [45] found them to be substantial. However, in  $(\text{TMTSF})_2\text{ReO}_4$ , the DKC oscillations are extremely weak and almost invisible [45]. This dramatic difference in manifestations of AMRO in the three materials requires a theoretical explanation.

When a magnetic field is rotated in the  $(y, z)$  plane at  $B_x = 0$ , the theoretical calculations cited above show that the Lebed peaks in  $\sigma_{zz}$  can exist only for those magic angles  $(n, m)$  where the interchain tunneling amplitudes in the directions  $n\mathbf{b} + m\mathbf{c}$  are present [24, 47]. It is reasonable to expect that the interplane tunneling amplitudes in  $(\text{TMTSF})_2\text{PF}_6$  exist between the nearest and next-nearest chains in the  $\mathbf{c}$  and  $\mathbf{c} \pm \mathbf{b}$  directions (see Fig. 1). This would explain why only the Lebed resonance with  $n = 0, \pm 1$  are observed in  $(\text{TMTSF})_2\text{PF}_6$ . However, many magic angles with big numbers  $n$  are observed in  $(\text{TMTSF})_2\text{ClO}_4$  and  $(\text{TMTSF})_2\text{ReO}_4$ . It is hard to imagine that direct electron overlap exists between the chains separated by 11 interchain distances.

One way to resolve this problem is to take into account the nonlinear electron dispersion along the chains. (All theoretical papers cited above make a linearized approximation for the electron dispersion along the chains.) The first attempt in this direction was made in Ref. [48], and a more systematic study was presented in Refs. [49, 50]. The nonlinearity can indeed generate an effect similar, albeit not completely equivalent, to presence of many interchain tunneling amplitudes. However, the nonlinearity alone is not sufficient to explain the differences in AMRO between the three compounds. Another problem is the absence of the DKC oscillations in  $(\text{TMTSF})_2\text{ReO}_4$ . One might think that quantum coherence is too low in this material, but the existence of 21 Lebed oscillations clearly refutes this idea [46]. We see that a detailed theoretical understanding of AMRO in the  $(\text{TMTSF})_2\text{X}$  materials is challenging and requires additional ideas.

We believe that the key to understanding of the differences in AMRO is the presence of anion ordering in  $(\text{TMTSF})_2\text{ClO}_4$  and  $(\text{TMTSF})_2\text{ReO}_4$  and its absence in  $(\text{TMTSF})_2\text{PF}_6$ .  $\text{PF}_6$  is an octagonal centrosymmetric anion, which does not experience any orientational ordering at low temperatures. In contrast,  $\text{ClO}_4$  and  $\text{ReO}_4$  are tetragonal anions without inversion symmetry. Because their crystal sites have inversion symmetry, these anions have two different orientations of the same energy. At low temperatures, the anions experience orientational ordering and produce crystal superstructures [1] with the wave vectors  $\mathbf{Q} = (0, 1/2, 0)$  in  $(\text{TMTSF})_2\text{ClO}_4$  (under ambient pressure) and  $\mathbf{Q} = (0, 1/2, 1/2)$  in  $(\text{TMTSF})_2\text{ReO}_4$  (under pressure greater than about 10 kbar), as shown in Fig. 1. Formation of a crystal superstructure affects electron spectrum by folding the Brillouin zone. In this paper, we show that reconstruction of the electron dispersion caused by the anion ordering generates effective tunneling amplitudes between many distant chains. This effect explains why many Lebedev angles are observed in  $(\text{TMTSF})_2\text{ReO}_4$  and  $(\text{TMTSF})_2\text{ClO}_4$ , but not in  $(\text{TMTSF})_2\text{PF}_6$ . It also explains why the magic angles (1) are observed only for odd  $n$  in  $(\text{TMTSF})_2\text{ReO}_4$  [46] and only for even  $n$  in  $(\text{TMTSF})_2\text{ClO}_4$  [4, 5] at  $m = 1$ . We also explain the differences in the DKC oscillations within the same framework.

In contrast to the previous theories of AMRO for the anion superstructure of  $(\text{TMTSF})_2\text{ClO}_4$  [26, 27, 30, 49], we take into account the direct effect of anion ordering on the interlayer tunneling amplitude, which is especially important for  $(\text{TMTSF})_2\text{ReO}_4$ . In this way, we can capture the characteristic features of AMRO in the three compounds without invoking the nonlinearity of the longitudinal electron dispersion [49, 50].

In the second part of the paper (Sec. VI), we study the effect of a strong magnetic field parallel to the layers. We show that, when  $B_y$  is strong enough and exceeds a certain threshold related to the anion gap  $E_g$ , the interlayer tunneling between different branches of the folded electron dispersion becomes possible, and  $\sigma_{zz}$  should increase sharply. Experimental observation of this effect would allow direct measurement of  $E_g$ . This effect can be also applied to study the interband tunneling in  $\kappa$ -(ET) $_2\text{Cu}(\text{NCS})_2$ . A theory of this effect cannot be formulated within the framework of quasiclassical orbits on a warped Fermi surface. We calculate interlayer conductivity in the presence of anion ordering using the quantum limit, where the electron wave functions are confined to the layers due to a strong parallel magnetic field [51, 52, 53, 54].

## II. CALCULATION OF INTERLAYER CONDUCTIVITY

The general form of the electron dispersion in a Q1D metal is

$$\varepsilon(\mathbf{k}) = \pm \hbar v_F (k_x \mp k_F) + \varepsilon_\perp(k_y, k_z), \quad (2)$$

where the energy  $\varepsilon$  is measured from the Fermi energy, and  $\mathbf{k} = (k_x, k_y, k_z)$  is the electron wave vector. Here we linearize the dispersion along the chains with the Fermi velocity  $v_F$  near the Fermi wave vectors  $\pm k_F$ . There are two sheets of the open Fermi surface, but we present calculations only for the sheet with  $+v_F$ . Since  $t_c \ll t_b$ , we can expand the transverse dispersion  $\varepsilon_\perp$  to the lowest order in the interlayer tunneling amplitude  $t_c$

$$\varepsilon_\perp(k_y, k_z) = 2t_b \varepsilon_y(k_y b) + 2t_c f(k_y b) \cos(k_z c). \quad (3)$$

For a simple model with electron tunneling between the nearest chains in the absence of a superstructure, Eq. (3) reduces to the standard tight-binding expression with  $\varepsilon_y(k_y) = \cos(k_y b)$  and  $f(k_y b) = 1$ . However, we will show in Secs. IV and V that a nontrivial function  $f(k_y b)$  appears in the interlayer tunneling term in the presence of anion ordering. This effect was not considered in previous literature and plays crucial role in our consideration.

From the dispersion relation (2), we obtain the electron velocity  $\mathbf{v} = \partial \varepsilon / \hbar \partial \mathbf{k}$

$$v_x = v_F, \quad v_y \approx \frac{2t_b}{\hbar} \frac{d\varepsilon_y}{dk_y}, \quad v_z = -\frac{2t_c c}{\hbar} f(k_y b) \sin(k_z c). \quad (4)$$

In the quasiclassical approximation, the time-dependent electron wave vector  $\mathbf{k}^{(t)}$  follows the equation of motion

$$\hbar \frac{d\mathbf{k}^{(t)}}{dt} = e v^{(t)} \times \mathbf{B}, \quad (5)$$

where  $e$  is the electron charge, and the magnetic field  $\mathbf{B}$  is in the SI units. Given that  $v_x = v_F \gg v_z$ , we find

$$\frac{dk_y^{(t)}}{dt} \approx -\frac{e v_F B_z}{\hbar}, \quad k_y^{(t)} = -\frac{\omega_c t}{b} + k_y^{(0)}, \quad \omega_c = \frac{e b v_F B_z}{\hbar}, \quad (6)$$

where  $\omega_c$  is the analog of the cyclotron frequency for the open Fermi surface. The equation of motion for  $k_z$  is

$$dk_z = \frac{e}{\hbar} \left( v_F B_y dt - \frac{2t_b B_x}{\hbar} \frac{d\varepsilon_y}{dk_y} dt \right). \quad (7)$$

Using  $dk_y/dt$  from Eq. (6), we get

$$ck_z^{(t)} = B'_y \omega_c t + B'_x \varepsilon_y(k_y^{(t)}) + ck_z^{(0)}, \quad (8)$$

where we introduced the dimensionless parameters

$$B'_y = \frac{B_y c}{B_z b}, \quad B'_x = \frac{B_x}{B_z} \frac{2t_b c}{\hbar v_F}. \quad (9)$$

The variables  $B'_y$  and  $B'_x$  are proportional to the tangents of the magnetic field projections onto the  $(y, z)$  and  $(x, z)$  planes, respectively.

The interlayer conductivity  $\sigma_{zz}$  is given by the Shockley tube integral [34]

$$\sigma_{zz} = \frac{4e^2}{\hbar} \iint \frac{dk_y^{(0)} dk_z^{(0)}}{(2\pi)^3 v_F} \int_{-\infty}^0 dt v_z(\mathbf{k}^{(0)}) v_z(\mathbf{k}^{(t)}) e^{t(1/\tau - i\omega)}, \quad (10)$$

where  $\tau$  is a relaxation time, and the factor 4 comes from the two spin projections and the two sheets of the Fermi surface. Substituting Eqs. (4), (6), and (8) into Eq. (10), we find the real part of  $\sigma_{zz}$

$$\sigma_{zz} = \frac{e^2 t_c^2 c}{\pi^2 \hbar^3 \omega_c v_F b} \mathcal{R}e \sum_{\mp} \int_0^{2\pi} d\phi \int_0^{\infty} d\eta f(\phi) f(\phi + \eta) \quad (11)$$

$$\times \exp\{iB'_x[\varepsilon_y(\phi) - \varepsilon_y(\phi + \eta)] - \eta[1/\omega_c \tau - iB'_y \mp i\omega/\omega_c]\},$$

where  $\phi = bk_y^{(0)}$  and  $\eta = -\omega_c t$ . Expanding the periodic functions  $f(\phi) e^{iB'_x \varepsilon(\phi)}$  in Eq. (11) into the Fourier series with the coefficients

$$A_n(B'_x) = \frac{1}{2\pi} \int_0^{2\pi} e^{-in\phi} f(\phi) e^{iB'_x \varepsilon_y(\phi)} d\phi, \quad (12)$$

we obtain

$$\frac{\sigma_{zz}}{\sigma_0} = \frac{1}{2} \sum_{\mp} \sum_{n=-\infty}^{\infty} \frac{|A_n(B'_x)|^2}{1 + (\omega_c \tau)^2 (n - B'_y \mp \omega/\omega_c)^2}. \quad (13)$$

Here  $\sigma_0 = (4e^2 t_c^2 \tau c)/(\pi \hbar^3 v_F b)$  is the interlayer dc conductivity at  $\mathbf{B} = 0$ , and the  $\pm$  terms represent contributions from the two sheets of the Fermi surface. In the rest of the paper, we shall focus on the dc conductivity  $\sigma_{zz}$  at  $\omega = 0$ , although Eq. (13) also gives the ac conductivity.

The Lebed effect corresponds to the resonant peaks of  $\sigma_{zz}$  in Eq. (13) achieved at  $B'_y = n$ , where the condition (1) for  $m = 1$  is satisfied. In a simple model without anion ordering, where  $\varepsilon_y = \cos(k_y b)$  and  $f = 1$ , Eq. (12) reduces to  $A_n(B'_x) = i^n J_n(B'_x)$ , where  $J_n$  is the Bessel function. In this case, Eq. (13) reproduces the result found in Refs. [25, 31, 35, 36, 37]. However, the coefficients  $J_n(B'_x)$  vanish for  $n \neq 0$  at  $B_x = 0$ , so there are no Lebed oscillations in this model for a magnetic field rotation in the  $(y, z)$  plane. The DKC effect originates from the oscillations of  $J_n(B'_x)$  vs.  $B'_x$  in the numerator of Eq. (13).

Interestingly, Eq. (13) with  $|A_n|^2 = J_n^2(B'_x)$  and  $\omega = 0$  is exactly the same as the equation that describes the Mach-Zehnder interference in a superconducting qubit driven by an ac electric field and subjected to a dc bias [38, 39]. The two states of the qubit correspond to the two adjacent layers of a Q1D conductor coupled by the tunneling amplitude  $t_c$ . The frequency of the ac field for the qubit maps to the frequency  $\omega_c$  in Eq. (6), the detuning of the qubit maps to  $B'_y \omega_c = ecv_F B_y/\hbar$ , and the amplitude of the ac modulation maps to  $B'_x$  in Eq. (9). The contour plot of Eq. (13) shown in Fig. 2 of Ref. [37] is exactly the same as in Refs. [38, 39] and represents the so-called Bessel staircase. The same equation also appears in the theory of laser cooling in ion traps [43]. This correspondence is not just a mathematical curiosity, but reflects profound similarity between these highly coherent quantum system, where the oscillatory patterns are caused by phase interference due to applied electric and magnetic fields.

### III. INTERLAYER CONDUCTIVITY IN (TMTSF)<sub>2</sub>PF<sub>6</sub> WITHOUT ANION ORDERING

Let us first discuss the case of (TMTSF)<sub>2</sub>PF<sub>6</sub>, which does not have anion ordering. In order to observe more than one Lebed angle, we need to introduce the tunneling amplitude  $t'_c$  between next-nearest neighboring chains, as shown in Fig. 1(b). Including this term in the transverse dispersion (3), we find for (TMTSF)<sub>2</sub>PF<sub>6</sub>

$$\varepsilon_y(\phi) = \cos \phi, \quad f(\phi) = 1 + 2 \frac{t'_c}{t_c} \cos \phi, \quad \phi = bk_y. \quad (14)$$

In a more general case, where the amplitudes  $t_n$  corresponding to the tunneling vectors  $\mathbf{c} + n\mathbf{b}$  are present, the transverse dispersion relation can be written as

$$\varepsilon_{\perp}(k_y, k_z) = 2t_b \cos(k_y b) + 2 \sum_l t_l \cos(k_z c + lk_y b). \quad (15)$$

Eq. (14) is the special case of Eq. (15) with  $t_0 = t_c$  and  $t_{\pm 1} = t'_c$ .

Generalizing the derivation presented in Sec. II to the transverse dispersion relation (15), we find that the interlayer conductivity  $\sigma_{zz}$  is given by Eq. (13) with the following coefficients  $A_n$  [55]

$$A_n(B'_x) = \frac{1}{t_c} \sum_l i^{n+l} t_l J_{n+l}(B'_x). \quad (16)$$

In the case of (TMTSF)<sub>2</sub>PF<sub>6</sub>, Eqs. (12) and (14) or Eq. (16) give

$$A_n(B'_x) = i^n J_n(B'_x) + i^{n+1} \frac{t'_c}{t_c} J_{n+1}(B'_x) + i^{n-1} \frac{t'_c}{t_c} J_{n-1}(B'_x). \quad (17)$$

Substituting Eq. (17) into Eq. (13), we find the following results for AMRO in (TMTSF)<sub>2</sub>PF<sub>6</sub>.

When  $B'_x = 0$ , i.e. we consider a magnetic field rotation in the  $(y, z)$  plane, only the terms with  $n = 0$  and  $n = \pm 1$  have non-zero coefficients  $A_n$  in the sum in Eq. (13). These terms give rise to the Lebed peaks at  $n = 0$  and  $n = \pm 1$  with the heights proportional to  $t_c^2$  and  $(t'_c)^2$ .

When we consider the DKC oscillations at  $B'_y = 0$ , i.e. for a magnetic field rotation in the  $(x, z)$  plane, the sum in Eq. (13) is dominated by the term with  $n = 0$ , because the other terms have the big factor  $(\omega_c \tau)^2$  in the denominator. Keeping only the term with  $n = 0$  and using Eq. (17), we can write approximately

$$\frac{\sigma_{zz}(B'_x)}{\sigma_0} \approx \left| J_0(B'_x) + 2i \frac{t'_c}{t_c} J_1(B'_x) \right|^2. \quad (18)$$

When  $t'_c = 0$ , Eq. (18) vanishes for the angles where  $J_0(B'_x) = 0$ , which is a manifestation of the DKC oscillations. However, in the presence of  $t'_c \neq 0$ , Eq. (18) does not vanish for any angles, so the DKC oscillations are partially suppressed, although some modulation of  $\sigma_{zz}$  vs.  $B'_x$  remains. We see that the presence of tunneling amplitudes  $t_l$  to more distant chains enhances the Lebed oscillations, but suppresses the DKC oscillations. This conclusion was already made in Ref. [37].

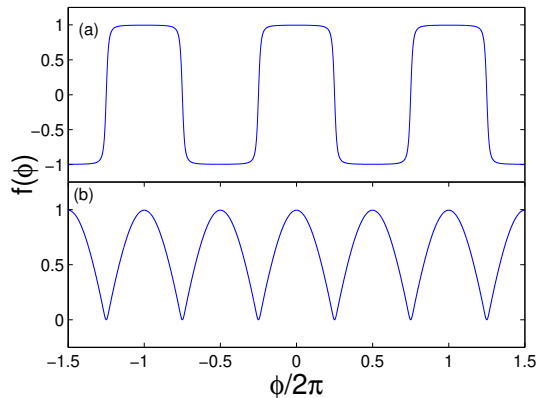


FIG. 2: (a) Plot of the function  $f(\phi)$  given by Eq. (22). (b) Plot of the second term in  $f(\phi)$  given by Eq. (25). In both plots,  $E_g/2t_b = 0.1$ .

#### IV. ANION ORDERING IN $(\text{TMTSF})_2\text{ReO}_4$

The  $\text{ReO}_4$  anions order with the wave vector  $\mathbf{Q} = (0, 1/2, 1/2)$  under pressure. This causes the energies of the odd and even chains to split by  $\pm E_g$ , as illustrated in Fig. 1(a). The Hamiltonian of interchain tunneling is described by a  $2 \times 2$  matrix representing the even and odd chains [56]:

$$H_{\perp} = \begin{pmatrix} E_g & 2t_b \cos(k_y b) + 2t_c \cos(k_z c) \\ \text{c.c.} & -E_g \end{pmatrix}. \quad (19)$$

The eigenvalues of the matrix (19) give the transverse electron dispersion relation

$$\varepsilon_{\perp} = \pm \sqrt{[2t_b \cos(k_y b) + 2t_c \cos(k_z c)]^2 + E_g^2}. \quad (20)$$

Expanding Eq. (20) to the zeroth and first order in  $t_c$ , we find the functions  $\varepsilon_y(k_y)$  and  $f(k_y)$  in Eq. (3)

$$\varepsilon_y(\phi) = \pm \sqrt{\cos^2 \phi + (E_g/2t_b)^2}, \quad \phi = bk_y, \quad (21)$$

$$f(\phi) = \pm \frac{\cos \phi}{\sqrt{\cos^2 \phi + (E_g/2t_b)^2}}. \quad (22)$$

The function  $f(\phi)$  (22) is close to a square wave for  $E_g/t_b \ll 1$ , as shown in Fig. 2(a). Its Fourier coefficients  $A_n$ , given by Eq. (12) with  $B'_x = 0$ , are non-zero only for odd  $n$  and decay as  $1/n$ . Transforming Eq. (3) from the momentum space to the real space, we find that the Fourier coefficients of  $f(k_y b)$  generate effective interplane tunneling amplitudes along the vectors  $\mathbf{c} + n\mathbf{b}$  with odd  $n$ , which are shown in Fig. 1(a) by the arrows. Initially, the model has only the tunneling amplitudes  $t_b$  and  $t_c$  between the nearest chains, but the anion ordering generates effective tunneling amplitudes between many chains. The higher-order expansion of Eq. (20) in  $t_c$  would generate effective tunneling amplitudes along

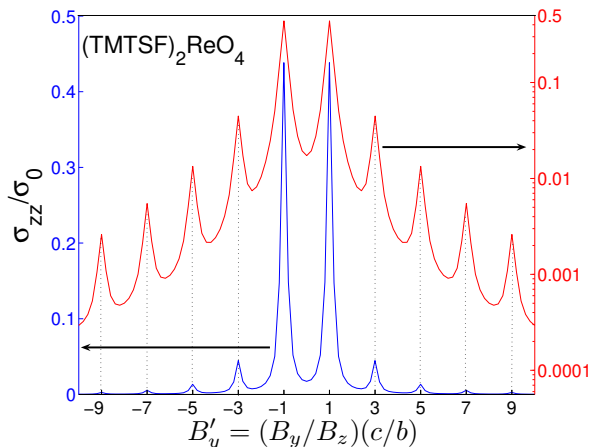


FIG. 3: Normalized interlayer conductivity  $\sigma_{zz}/\sigma_0$  calculated from Eq. (13) for  $(\text{TMTSF})_2\text{ReO}_4$  and plotted vs.  $B'_y$  at  $B'_x = 0$ , shown in the linear (left) and logarithmic (right) scales.

the vectors  $m\mathbf{c} + n\mathbf{b}$  with  $m$  and  $n$  of the same parity between the sites of the same type, either open circles or closed circles in Fig. 1(a). However, one should keep in mind that this heuristic real-space picture [46] is an oversimplification, and an accurate calculation in the momentum space should be performed as described above.

In Fig. 3 we show the normalized dc conductivity calculated from Eq. (13) for  $B'_x = 0$  and  $\omega_c\tau = \sqrt{50}$  using the Fourier coefficients  $A_n$  from Eq. (12). Since  $A_n \neq 0$  only for odd  $n$ , therefore  $\sigma_{zz}$  has peaks only at the odd Lebed angles, as shown in Fig. 3 and observed in  $(\text{TMTSF})_2\text{ReO}_4$  [46]. The higher-order expansion of Eq. (20) in  $t_c$  would generate peaks at the Lebed magic angles with  $m$  and  $n$  of the same parity in Eq. (1), as observed in Ref. [46]. Because of the anion superstructure, Eq. (20) is highly non-linear in  $\cos \phi$ , so its Fourier expansion generates a big number of harmonics, which produce a big number of Lebed peaks in AMRO. This is the qualitative reason why so many Lebed peaks are observed in  $(\text{TMTSF})_2\text{ReO}_4$ , in contrast to  $(\text{TMTSF})_2\text{PF}_6$ , which has no anion superstructure.

Fig. 4 shows a contour plot of  $\ln(\sigma_{zz}/\sigma_0)$  vs.  $B'_x$  and  $B'_y$ , as calculated from Eq. (13) using Eqs. (12), (21), and (22). The conductivity is maximal at the vertical lines corresponding to the odd Lebed magic angles. At a fixed Lebed angle, the weak modulation of  $\sigma_{zz}$  vs.  $B'_x$  (along a vertical line) corresponds to the DKC oscillations. Fig. 4 shows that the DKC oscillations are very weak, because the coefficients  $A_n(B'_x)$  (12) do not have zeros vs.  $B'_x$  in the presence of anion ordering, unlike the Bessel functions  $J_n(B'_x)$  in a simple model. This is a theoretical explanation of why the DKC oscillations in  $(\text{TMTSF})_2\text{ReO}_4$  are very weak and barely detectable experimentally [46].

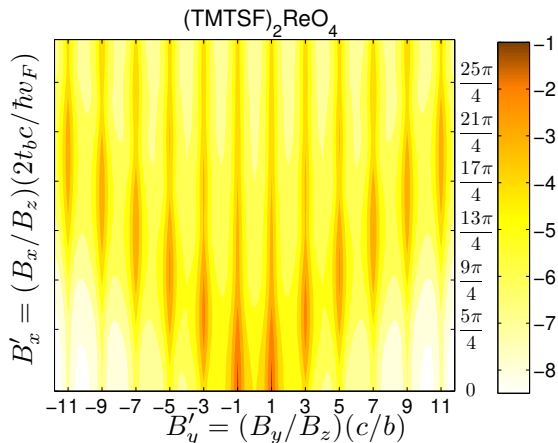


FIG. 4: Contour plot of  $\ln(\sigma_{zz}/\sigma_0)$  calculated from Eq. (13) for  $(\text{TMTSF})_2\text{ReO}_4$  at  $\omega_c\tau = \sqrt{50}$ .

## V. ANION ORDERING IN $(\text{TMTSF})_2\text{ClO}_4$

In the case of  $(\text{TMTSF})_2\text{ClO}_4$ , in order to observe multiple Lebed angles, we need to take into account the tunneling amplitude  $t'_c$  introduced in Sec. III and shown in Fig. 1(b). For the anion ordering with  $\mathbf{Q} = (0, 1/2, 0)$ , the interchain tunneling is described by the Hamiltonian

$$H_{\perp} = \begin{pmatrix} E_g + 2t_c \cos(k_z c) & \cos(k_y b)[2t_b + 4t'_c \cos(k_z c)] \\ \text{c.c.} & -E_g + 2t_c \cos(k_z c) \end{pmatrix}. \quad (23)$$

The eigenvalues of the matrix (23) give the transverse electron dispersion relation

$$\varepsilon_{\perp} = 2t_c \cos(k_z c) \pm \sqrt{\cos^2(k_y b)[2t_b + 4t'_c \cos(k_z c)]^2 + E_g^2}. \quad (24)$$

Expanding Eq. (24) to the zeroth and first order in  $t_c$  and comparing with Eq. (3), we find  $\varepsilon_y(\phi)$  to be the same as in Eq. (21) and

$$f(\phi) = 1 \pm \frac{t'_c}{t_c} \frac{2 \cos^2 \phi}{\sqrt{\cos^2 \phi + (E_g/2t_b)^2}}. \quad (25)$$

Only the second term in Eq. (25) generates the coefficients  $A_n$  with  $n \neq 0$  when substituted into Eq. (12) at  $B_x = 0$ . For  $E_g/t_b \ll 1$ , this term is close to a rectified cosine signal, as shown in Fig. 2(b), and its Fourier coefficients decay as  $1/n^2$  for large  $n$ . It has non-zero Fourier coefficients only for even  $n$ , thus  $\sigma_{zz}$  vs.  $B'_y$  has peaks at the even Lebed angles, as shown in Fig. 5 for  $B'_x = 0$  and observed experimentally in  $(\text{TMTSF})_2\text{ClO}_4$  [4, 5]. Because the second term in Eq. (25) is highly nonlinear in  $\cos \phi$ , it generates many harmonics and many Lebed peaks. However, they decay with the increase of  $n$  faster in  $(\text{TMTSF})_2\text{ClO}_4$  than in  $(\text{TMTSF})_2\text{ReO}_4$ . Moreover, because  $t'_c$  is small, the Lebed oscillations in  $(\text{TMTSF})_2\text{ClO}_4$  are weak, in agreement with the observations in Refs. [4, 5, 45]. As discussed in Sec. III, the DKC oscillations are controlled by the coefficient  $A_0(B'_x)$

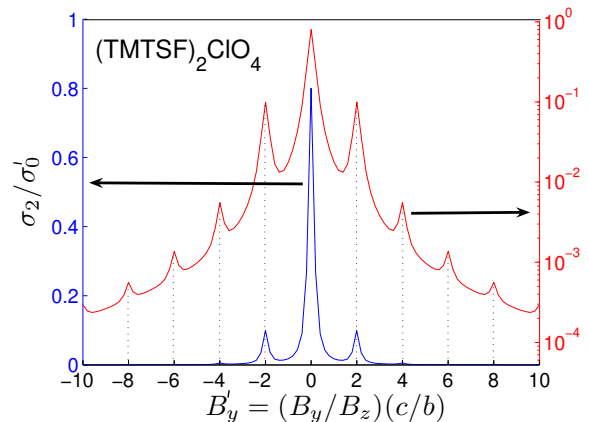


FIG. 5: Plot of  $\sigma_2/\sigma'_0$  vs.  $B'_y$  at  $B'_x = 0$ , shown in the linear (left) and logarithmic (right) scales.  $\sigma_2$  is the contribution to  $\sigma_{zz}$  in Eq. (13) from the second term in Eq. (25), and  $\sigma'_0 = \sigma_0(t'_c/t_c)^2$ .

in Eq. (13). The first term in Eq. (25) gives the main contribution to  $A_0(B'_x)$ , proportional to  $J_0(B'_x)$ . Thus, the DKC oscillations are relatively strong in  $(\text{TMTSF})_2\text{ClO}_4$ , as observed in Refs. [8, 45], although they are somewhat reduced by the second term in Eq. (25).

We conclude that the different types of anion ordering in  $(\text{TMTSF})_2\text{ReO}_4$  and  $(\text{TMTSF})_2\text{ClO}_4$  can indeed explain the characteristic features of AMRO in these materials. In  $(\text{TMTSF})_2\text{ReO}_4$ , the Lebed oscillations are strong and numerous, but the DKC oscillations are very weak. In  $(\text{TMTSF})_2\text{ClO}_4$ , the Lebed oscillations are numerous, but weak, whereas the DKC oscillations are relatively strong. On the other hand, there is no anion superstructure in  $(\text{TMTSF})_2\text{PF}_6$ . This material exhibits a few, but strong, Lebed oscillations and partially suppressed DKC oscillations.

## VI. INTERBAND TUNNELING IN A STRONG MAGNETIC FIELD PARALLEL TO THE LAYERS

Folding of the Brillouin zone due to anion ordering produces two branches (or two bands) of the electron dispersion, which we label by the index  $\alpha = \pm$  according to the sign in Eq. (21). The Fermi surfaces of the two bands, obtained from Eq. (2), are shown by the two solid lines in Fig. 6 for  $E_g/t_b = 0.1$ . (This picture is for the Fermi surface sheets near  $+k_F$ .)

In this Section, we study interlayer conductivity in a strong magnetic field  $(B_x, B_y, 0)$  parallel to the layers. We use the formalism developed in Refs. [35, 36, 37] and calculate  $\sigma_{zz}$  between just two layers, i.e. for a bilayer. Assuming that  $t_c$  is very weak, one can argue that, in the lowest order in  $t_c$ , the interlayer conductivity of a bulk multilayer crystal is determined by the interlayer conductivity between a pair of layers [56].

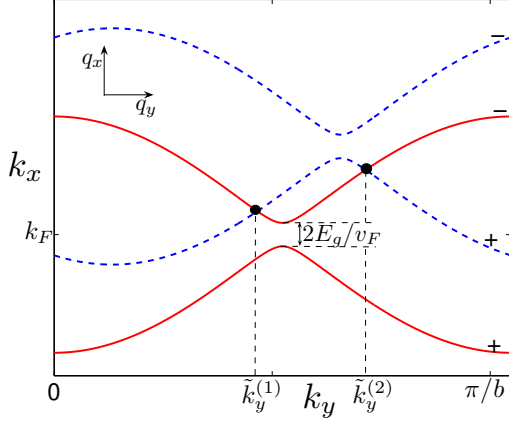


FIG. 6: Fermi surfaces of two adjacent layers shifted by the vector  $\mathbf{q}$  of Eq. (28) due to an in-plane magnetic field. The Fermi surfaces for each layer (the solid lines and the dashed lines) consist of two bands separated by the gap  $2E_g/v_F$  due to anion ordering and labeled + and -.

The tunneling Hamiltonian between layers 1 and 2 is

$$\hat{H}_c = t_c \int \hat{\psi}_2^\dagger(\mathbf{r}) \hat{\psi}_1(\mathbf{r}) e^{i\chi(\mathbf{r})} d^2r + \text{H.c.}, \quad (26)$$

$$\chi(\mathbf{r}) = \frac{ec}{\hbar} A_z(\mathbf{r}), \quad A_z(\mathbf{r}) = B_x y - B_y x, \quad (27)$$

where  $\hat{\psi}_{1,2}$  are the electron destruction operators in the layers 1 and 2. Here  $A_z$  is the vector potential of the in-plane magnetic field, and  $\chi(\mathbf{r})$  is the corresponding gauge phase accumulated in the process of tunneling across the interlayer spacing  $c$ . Substituting Eq. (27) into Eq. (26) and using momentum representation in the  $(x, y)$  plane, we observe that the in-plane wave vector of the electron changes from  $\mathbf{k}$  to  $\mathbf{k} + \mathbf{q}$  in the process of tunneling [37], where the vector  $\mathbf{q}$  is

$$\mathbf{q} = (q_x, q_y) = \frac{ec}{\hbar} (B_y, -B_x). \quad (28)$$

Thus, the Fermi surfaces of the second layer are shifted by the vector  $\mathbf{q}$  relative to the Fermi surfaces of the first layer as shown by the two dashed lines in Fig. 6. A similar picture was discussed for closed Fermi surfaces in semiconducting bilayers in Refs. [35, 57, 58, 59].

The interlayer conductivity  $\sigma_{zz}^{\alpha\beta}$  between the bands  $\alpha$  and  $\beta$  is given by the following expression [35, 60]

$$\sigma_{zz}^{\alpha\beta} = \frac{e^2 t_c^2 c}{\hbar \pi} \sum_{\mathbf{k}} |M_{\alpha\beta}|^2 S(\mathbf{k}, E_F) S(\mathbf{k} + \mathbf{q}, E_F), \quad (29)$$

where  $M_{\alpha\beta} = \langle \psi_{\alpha}^{(2)}(\mathbf{k} + \mathbf{q}) | \psi_{\beta}^{(1)}(\mathbf{k}) \rangle$  is the scalar product between the in-plane electron wave functions belonging to adjacent layers. These matrix elements are discussed in more detail in Appendix A. The total interlayer conductivity is the sum over all bands  $\sigma_{zz} = \sum_{\alpha\beta} \sigma_{zz}^{\alpha\beta}$ . The function  $S(\mathbf{k}, E_F)$  is the spectral density of the in-plane

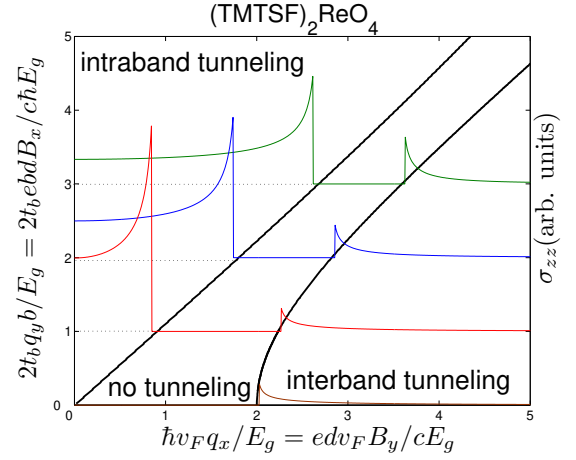


FIG. 7: Phase diagram of interlayer tunneling vs. the normalized in-plane magnetic field components  $B_y$  and  $B_x$ . Tunneling between the same and different types of bands is possible in the upper left and the lower right regions of the diagram, correspondingly, and not possible in the intermediate region. The thin curves show the interlayer conductivity  $\sigma_{zz}$  calculated using Eq. (34) as a function of  $B_y$  for several values of  $B_x$  for the superstructure of  $(\text{TMTSF})_2\text{ReO}_4$ .

electron Green function evaluated at the Fermi energy  $E_F$  as a function of the wave vector  $\mathbf{k}$  [35, 60]

$$S(\mathbf{k}, E_F) = \frac{2\Gamma}{[E_F - \varepsilon(\mathbf{k})]^2 + \Gamma^2}, \quad (30)$$

where  $\Gamma = \hbar/2\tau$  is the relaxation rate, and  $\varepsilon(\mathbf{k})$  is the electron dispersion within the layer.

When  $\Gamma$  is small, i.e., when the electron quasiparticles have a long lifetime time  $\tau$ , the spectral function (30) can be replaced by a delta function:  $S(\mathbf{k}, E_F) \approx 2\pi\delta[E_F - \varepsilon(\mathbf{k})]$ . Substituting this expression into Eq. (29), we find

$$\sigma_{zz}^{\alpha\beta} = \frac{e^2 t_c^2 c |\tilde{M}_{\alpha\beta}|^2}{\hbar \pi} \iint dk_y dk_x \delta[\hbar v_F k_x + \alpha 2t_b \varepsilon_y(k_y b)] \times \delta[\hbar v_F(k_x - q_x) + \beta 2t_b \varepsilon_y(k_y b - q_y b)], \quad (31)$$

where the matrix element  $\tilde{M}_{\alpha\beta}$  is evaluated at the points where both delta functions are satisfied. Integrating Eq. (31) over  $k_x$ , we find

$$\sigma_{zz}^{\alpha\beta} = \frac{e^2 t_c^2 c |\tilde{M}_{\alpha\beta}|^2}{\pi \hbar^2 v_F} \int dk_y \delta[g_{\alpha\beta}(k_y)], \quad (32)$$

where the function  $g_{\alpha\beta}(k_y)$  is

$$g_{\alpha\beta}(k_y) = v_F q_x + 2t_b [\alpha \varepsilon_y(k_y b) - \beta \varepsilon_y(k_y b - q_y b)]. \quad (33)$$

Taking the integral (32), we find

$$\sigma_{zz}^{\alpha\beta} = \frac{e^2 t_c^2 c}{\pi \hbar^2 v_F} \sum_{\tilde{k}_y} \frac{|M_{\alpha\beta}(\tilde{k}_y)|^2}{|\partial g_{\alpha\beta} / \partial k_y|}, \quad (34)$$

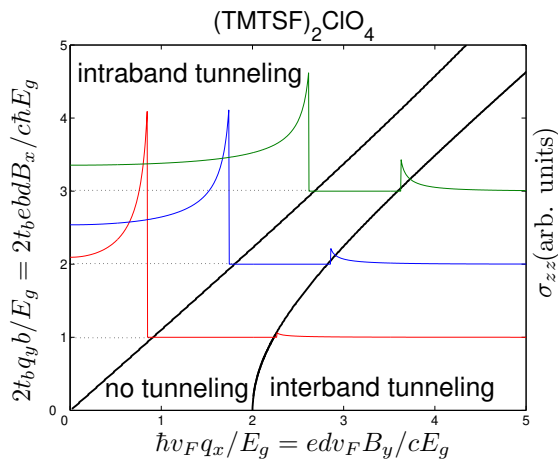


FIG. 8: The same as in Fig. 7, but for the superstructure of  $(\text{TMTSF})_2\text{ClO}_4$ .

where the sum is taken over the points  $\tilde{k}_y$  where the equation  $g_{\alpha\beta}(\tilde{k}_y) = 0$  is satisfied. Notice that the relaxation time  $\tau$  drops out from Eq. (34), so  $\sigma_{zz}$  should be temperature-independent in a strong parallel magnetic field [35].

Eq. (31) shows that a non-zero contribution to interlayer conductivity comes from the points where both delta functions are satisfied, i.e., the initial and final states belong to the Fermi surfaces of different layers. Geometrically, these are the intersection points  $\tilde{k}_y^{(1)}$  and  $\tilde{k}_y^{(2)}$  of the solid and dashed lines in Fig. 6. Depending on which Fermi surfaces intersect in Fig. 6, electrons can tunnel between different bands  $\alpha, \beta = \pm$  in the folded Brillouin zone. The equation  $g_{\alpha\beta}(\tilde{k}_y) = 0$  has solutions only in some regions of the  $(q_x, q_y)$  space, as shown by the thick solid lines in Figs. 7 and 8. Above the diagonal line in Figs. 7 and 8, the interlayer tunneling is possible only between the bands of the same type  $\alpha = \beta$ . If  $q_x$  exceeds the threshold value

$$\hbar v_F q_x = B_y e c v_F \geq 2E_g, \quad (35)$$

the interlayer tunneling between different bands,  $\alpha = -\beta$ , becomes possible in the lower right region in Figs. 7 and 8. No interlayer tunneling is possible in the intermediate region in Figs. 7 and 8, where the shifted Fermi surfaces in Fig. 6 do not cross. The boundaries of the regions are determined by the condition that the displaced Fermi surface touches the other one.

The plots of the interlayer conductivity  $\sigma_{zz}$ , calculated from Eq. (34), are shown in Figs. 7 and 8 as functions of  $B_y \propto q_x$  for several fixed values of  $B_x \propto q_y$ . We observe that the interlayer conductivity vanishes in the intermediate region and has peaks at the boundaries. The peaks originate from the increase of the phase volume in the integral (31) when the two Fermi surfaces touch each other. Fig. 7 corresponds to the anion superstructure of  $(\text{TMTSF})_2\text{ReO}_4$ . We observe that, when the magnetic

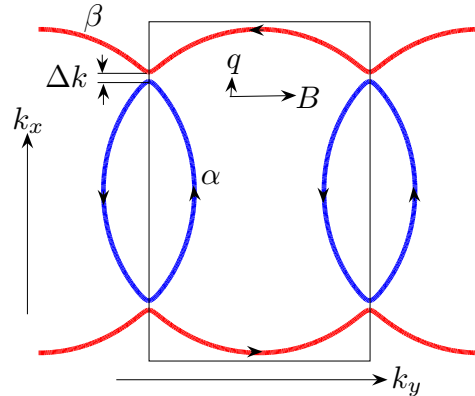


FIG. 9: The in-plane Fermi surface of  $\kappa\text{-(ET)}_2\text{Cu(NCS)}_2$ . The  $\alpha$  and  $\beta$  branches of the Fermi surface are separated by the distance  $\Delta k$  in the momentum space.

field is applied along the  $y$  axis ( $B_x = 0$ ), the interlayer conductivity  $\sigma_{zz}(B_y)$  is strongly suppressed until  $B_y$  exceeds the threshold, and then  $\sigma_{zz}$  increases sharply. The value of  $E_g$  can be determined from the measured threshold field  $B_y$  via Eq. (35). Fig. 8 corresponds to the anion superstructure of  $(\text{TMTSF})_2\text{ClO}_4$ . In this case, the eigenfunctions of different bands  $\alpha = -\beta$  are orthogonal, so the matrix element  $M_{-+}$  vanishes for  $q_y = 0$  (see Appendix A). Thus, in order to get a nonzero interlayer conductivity in  $(\text{TMTSF})_2\text{ClO}_4$ , it is necessary to have a non-zero component  $B_x \neq 0$ , so that  $q_y \neq 0$ .

According to the measurements in Ref. [18], the Fermi velocity in  $(\text{TMTSF})_2\text{ClO}_4$  is  $v_F \approx 10^5$  m/s. Substituting this value and the interlayer distance  $c = 1.35$  nm [1] into Eq. (35) and using the maximal stationary field of 45 T available at NHMFL in Tallahassee, we find the maximal anion gap  $2E_g \approx 70$  K that can be probed using this method. Various estimates of  $E_g$  are reviewed in Ref. [61]. Refs. [27, 62] estimated  $E_g$  as  $40 \div 50$  K, so the field of 45 T may be sufficient to exceed the threshold (35) at the ambient pressure. The experiment can be also performed in pulsed fields or under pressure, where the anion superstructure is progressively suppressed [63]. Measurements of the interlayer conductivity using pulsed magnetic fields of 46 T were performed in  $(\text{TMTSF})_2\text{ClO}_4$  [64], but the field was applied close to the  $x$  axis, rather than the  $y$  axis, as required for our effect.

A similar analysis can be also applied to the material  $\kappa\text{-(ET)}_2\text{Cu(NCS)}_2$ , whose in-plane Fermi surface is shown in Fig. 9. The separation  $\Delta k$  between the  $\alpha$  and  $\beta$  branches of the Fermi surface can be measured by applying an in-plane magnetic field in the horizontal direction in Fig. 9. This field shifts the Fermi surface of one layer by the vector  $\mathbf{q}$  shown in Fig. 9. The threshold magnetic field, at which the  $\alpha$  branch in one layer starts to touch the  $\beta$  branch in the other layer, can be calculated from

Eq. (28). Using  $\Delta k = 0.17 \text{ nm}^{-1}$  and the interlayer distance  $c = 1.62 \text{ nm}$  [1, 65], we estimate that the threshold magnetic field is of the order of 430 T, which is beyond the current experimental capabilities.

## VII. CONCLUSIONS

We have shown that the modifications of the electron dispersion due to the anion ordering in  $(\text{TMTSF})_2\text{ReO}_4$  and  $(\text{TMTSF})_2\text{ClO}_4$  generate effective tunneling amplitudes between many distant chains. These amplitudes cause peaks in the interlayer conductivity  $\sigma_{zz}$  at many Lebed magic angles (1). The different wave vectors of the anion ordering,  $\mathbf{Q} = (0, 1/2, 1/2)$  in  $(\text{TMTSF})_2\text{ReO}_4$  and  $\mathbf{Q} = (0, 1/2, 0)$  in  $(\text{TMTSF})_2\text{ClO}_4$ , result in the odd and even Lebed magic angles, as observed experimentally [46, 63]. Our theory also explains why the Lebed oscillations are strong and the DKC oscillations are weak in  $(\text{TMTSF})_2\text{ReO}_4$ , and vice versa in  $(\text{TMTSF})_2\text{ClO}_4$ , as observed experimentally [45].

When a strong magnetic field is applied parallel to the layers, and  $B_y$  exceeds a certain threshold, then interlayer tunneling between different branches of the Fermi surface, produced by folding of the Brillouin zone, should become possible. This effect would be observed as a sharp increase of interlayer conductivity. It can be utilized for a direct measurement of the anion gap  $E_g$ . Theoretical description of this effect required a quantum-mechanical treatment of the wave functions confined to different layers and cannot be achieved within the framework of quasiclassical electron orbits on a warped Fermi surface.

Experimental observation of the high number of magic angles (up to 21 in Ref. [46]) demonstrates a very high level of quantum coherence achieved in the Q1D organic conductors at low temperatures. This is remarkable given that the  $(\text{TMTSF})_2X$  materials have strong electron interactions. In different parts of their rich phase diagram, these materials have the Mott insulating phase and other exotic phases [1, 2]. It would be very interesting to study what happens to AMRO when the system is driven toward the Mott state using pressure or other variables.

We point out that the theory of the angular magnetoresistance oscillations (AMRO) in Q1D conductors is equivalent to the mathematical description of the Mach-Zehnder interference in a driven superconducting qubit [38, 39] and of laser cooling in ion traps [43]. Thus, the physics of Q1D conductors may have applications in quantum engineering well beyond the domain of solid-state material science.

## Acknowledgments

VMY is grateful for discussions with W. Kang, S. Hill, M.J. Naughton, S. Uji, W.D Oliver, S. Ashhab, and e-mail communications with A.G. Lebed and L. Levitov.

## APPENDIX A: CALCULATION OF THE MATRIX ELEMENTS

In this Appendix, we calculate the matrix elements of interlayer tunneling introduced in Eq. (29).

In the case of  $(\text{TMTSF})_2\text{ClO}_4$ , the interlayer tunneling with the amplitude  $t_c$  occurs between the chains of the same type, as shown in Fig. 1(b) [56]. The in-plane Hamiltonians of two adjacent layers are given by the same expression

$$\hat{H} = \begin{pmatrix} E_g & 2t_b \cos(k_y b) \\ 2t_b \cos(k_y b) & -E_g \end{pmatrix}. \quad (\text{A1})$$

The eigenvalues  $\lambda_{\pm}$  and the eigenvectors  $|\psi_{\pm}\rangle$  of the Hamiltonian (A1) are

$$\lambda_{\pm} = \pm \sqrt{[2t_b \cos(k_y b)]^2 + E_g^2}, \quad (\text{A2})$$

$$|\psi_{\pm}(k_y)\rangle = \frac{1}{N_{\pm}} (\lambda_{\pm} + E_g, 2t_b \cos k_y b), \quad (\text{A3})$$

$$N_{\alpha} = \sqrt{[2t_b \cos(k_y b)]^2 + (\lambda_{\alpha} + E_g)^2}. \quad (\text{A4})$$

The matrix elements of tunneling are proportional to the scalar products of the wave functions in adjacent layers:

$$M_{--} = \langle \psi_{-}(k_y + q_y) | \psi_{-}(k_y) \rangle, \quad (\text{A5})$$

$$M_{++} = \langle \psi_{+}(k_y + q_y) | \psi_{+}(k_y) \rangle \quad (\text{A6})$$

for tunneling between the same kinds of bands and

$$M_{-+} = \langle \psi_{-}(k_y + q_y) | \psi_{+}(k_y) \rangle \quad (\text{A7})$$

between different kinds of bands. It is clear from Eq. (A7) that  $M_{-+}$  vanishes for  $q_y = 0$  because  $|\psi_{+}(k_y)\rangle$  and  $|\psi_{-}(k_y)\rangle$  are orthogonal.

In the case of  $(\text{TMTSF})_2\text{ReO}_4$ , the inter-layer tunneling with the amplitude  $t_c$  occurs between the chains of different types. The in-plane Hamiltonian of one layer has the form (A1), whereas the sign of  $E_g$  is reversed in the Hamiltonian  $H'$  of another layer

$$H' = \begin{pmatrix} -E_g & 2t_b \cos(k_y b) \\ 2t_b \cos(k_y b) & E_g \end{pmatrix}. \quad (\text{A8})$$

The eigenvalues of  $H'$  are the same as in Eq. (A2), but the corresponding eigenvectors are different

$$|\psi'_{\pm}(k_y)\rangle = \frac{1}{N'_{\pm}} (\lambda_{\pm} - E_g, 2t_b \cos k_y b), \quad (\text{A9})$$

$$N'_{+} = N_{-}, \quad N'_{-} = N_{+}. \quad (\text{A10})$$

The scalar products of the wave functions in the adjacent layers now are

$$M_{--} = \langle \psi'_{-}(k_y + q_y) | \psi_{-}(k_y) \rangle, \quad (\text{A11})$$

$$M_{++} = \langle \psi'_{+}(k_y + q_y) | \psi_{+}(k_y) \rangle \quad (\text{A12})$$

for the same kinds of bands and

$$M_{-+} = \langle \psi'_{-}(k_y + q_y) | \psi_{+}(k_y) \rangle \quad (\text{A13})$$

for different kinds of bands. Now  $M_{-+}$  does not vanish for  $q_y = 0$ , because  $|\psi_{+}(k_y)\rangle$  and  $|\psi'_{-}(k_y)\rangle$  are not orthogonal.

- 
- [1] T. Ishiguro, K. Yamaji, and G. Saito, *Organic Superconductors* (Springer, Berlin, 1998).
- [2] *Physics of Organic Superconductors and Conductors*, edited by A.G. Lebed (Springer, Berlin, 2008).
- [3] A.G. Lebed, JETP Letters **43**, 174 (1986); A.G. Lebed and P. Bak, Phys. Rev. Lett. **63**, 1315 (1989).
- [4] T. Osada *et al.*, Phys. Rev. Lett. **66**, 1525 (1991).
- [5] M.J. Naughton *et al.*, Phys. Rev. Lett. **67**, 3712 (1991).
- [6] W. Kang, S.T. Hannahs, and P.M. Chaikin, Phys. Rev. Lett. **69**, 2827 (1992); E.I. Chashechkina and P.M. Chaikin, *ibid.* **80**, 2181 (1998); D.G. Clarke *et al.*, Science **279**, 2071 (1998).
- [7] K. Behnia, M. Ribault, and C. Lenoir, Europhys. Lett. **25**, 285 (1994).
- [8] G.M. Danner, W. Kang, and P.M. Chaikin, Phys. Rev. Lett. **72**, 3714 (1994).
- [9] G.M. Danner and P.M. Chaikin, Phys. Rev. Lett. **75**, 4690 (1995).
- [10] H. Yoshino *et al.*, J. Phys. Soc. Jpn. **64**, 2307 (1995); **66**, 2248 (1997); **66**, 2410 (1997).
- [11] T. Osada, S. Kagoshima, and N. Miura, Phys. Rev. Lett. **77**, 5261 (1996).
- [12] A.G. Lebed and N.N. Bagmet, Phys. Rev. B **55**, R8654 (1997).
- [13] I.J. Lee and M.J. Naughton, Phys. Rev. B **57**, 7423 (1998).
- [14] I.J. Lee and M.J. Naughton, Phys. Rev. B **58**, R13343 (1998).
- [15] W. Kang, T. Osada, Y.J. Jo, and H. Kang, Phys. Rev. Lett. **99**, 017002 (2007).
- [16] W. Kang, Phys. Rev. B **76**, 193103 (2007).
- [17] A. Ardavan *et al.*, Phys. Rev. Lett. **81**, 713 (1998); A.E. Kovalev, S. Hill, and J.S. Qualls, Phys. Rev. B **66**, 134513 (2002); Y. Oshima *et al.*, *ibid.* **68**, 054526 (2003); S. Takahashi *et al.*, J. Appl. Phys. **93**, 8665 (2003).
- [18] S. Takahashi *et al.*, Phys. Rev. B **72**, 024540 (2005).
- [19] S. Hill, Phys. Rev. B **55**, 4931 (1997).
- [20] S.J. Blundell and J. Singleton, Phys. Rev. B **53**, 5609 (1996); S.J. Blundell, A. Ardavan, and J. Singleton, Phys. Rev. B **55**, R6129 (1997).
- [21] S. Takahashi *et al.*, J. Low Temp. Phys. **142**, 315 (2006).
- [22] S. Hill and S. Takahashi in [2], p. 457.
- [23] W. Wu *et al.*, Phys. Rev. Lett. **94**, 097004 (2005).
- [24] T. Osada, S. Kagoshima, and N. Miura, Phys. Rev. B **46**, 1812 (1992).
- [25] A.G. Lebed and M.J. Naughton, Phys. Rev. Lett. **91**, 187003 (2003).
- [26] A.G. Lebed, H.I. Ha, and M.J. Naughton, Phys. Rev. B **71**, 132504 (2005).
- [27] H.I. Ha, A.G. Lebed, M.J. Naughton, Phys. Rev. B **73**, 033107 (2006).
- [28] T. Osada *et al.*, Synth. Metals **103**, 2024 (1999).
- [29] H. Yoshino and K. Murata, J. Phys. Soc. Jpn. **68**, 3027 (1999).
- [30] H. Yoshino *et al.*, J. Phys. Soc. Jpn. **68**, 3142 (1999).
- [31] K. Kobayashi, M. Saito, E. Ohmichi, and T. Osada, Phys. Rev. Lett. **96**, 126601 (2006).
- [32] W. Shockley, Phys. Rev. **79**, 191 (1950).
- [33] R.G. Chambers, Proc. Phys. Soc. A (London) **65**, 458 (1952).
- [34] J.M. Ziman, *Principles of Theory of Solids* (Cambridge University Press, Cambridge, 1972).
- [35] R.H. McKenzie, P. Moses, Phys. Rev. Lett. **81**, 4492 (1998); Phys. Rev. B **60**, 7998 (1999); U. Lundin and R.H. McKenzie, *ibid.* **70**, 235122 (2004).
- [36] T. Osada *et al.*, Synth. Metals **133–134**, 75 (2003); **135–136**, 653 (2003); Physica E **12**, 272 (2002); **18**, 200 (2003).
- [37] B.K. Cooper and V.M. Yakovenko, Phys. Rev. Lett. **96**, 037001 (2006).
- [38] W.D. Oliver *et al.*, Science **310**, 1653 (2005).
- [39] D.M. Berns *et al.*, Phys. Rev. Lett. **97**, 150502 (2006).
- [40] M. Sillanpää *et al.*, Phys. Rev. Lett. **96**, 187002 (2006).
- [41] A. Izmalkov *et al.*, Phys. Rev. Lett. **101**, 017003 (2008).
- [42] S. Ashhab, J.R. Johansson, A.M. Zagoskin, and F. Nori, Phys. Rev. A **75**, 063414 (2007).
- [43] R.G. DeVoe, J. Hoffnagle, and R.G. Brewer, Phys. Rev. A **39**, 4362 (1989); R. Blümel, C. Kappler, W. Quint, and H. Walther, Phys. Rev. A **40**, 808 (1989).
- [44] W. Wu, I.J. Lee, and P.M. Chaikin, Phys. Rev. Lett. **91**, 056601 (2003); N.P. Ong, W. Wu, P.M. Chaikin, and P.W. Anderson, Europhys. Lett. **66**, 579 (2004); W. Wu, N.P. Ong, and P.M. Chaikin, Phys. Rev. B **72**, 235116 (2005); E.S. Choi, J.S. Brooks, H. Kang, Y.J. Jo, and W. Kang, Phys. Rev. Lett. **95**, 187001 (2005); M.S. Nam, A. Ardavan, W. Wu, and P.M. Chaikin, Phys. Rev. B **74**, 073105 (2006); W. Wu and P.M. Chaikin, Phys. Rev. B **76**, 153102 (2007).
- [45] W. Kang, Y.J. Jo, and H.Y. Kang, J. Phys. Conference Series **51**, 355 (2006).
- [46] H. Kang *et al.*, Phys. Rev. B **68**, 132508 (2003).
- [47] E.I. Chashechkina and P.M. Chaikin, Phys. Rev. B **65**, 012405 (2001).
- [48] K. Maki, Phys. Rev. B **45**, R5111 (1992).
- [49] A.G. Lebed, N.N. Bagmet, and M.J. Naughton, Phys. Rev. Lett. **93**, 157006 (2004).
- [50] A.G. Lebed, N.N. Bagmet, and M.J. Naughton, J. Phys. IV France **114**, 77 (2004).
- [51] V.M. Yakovenko, Europhys. Lett. **3**, 1041 (1987); Sov. Phys. JETP **66**, 355 (1987).
- [52] V.M. Yakovenko, Phys. Rev. Lett. **61**, 2276 (1988).
- [53] A.G. Lebed, Phys. Rev. Lett. **95**, 247003 (2005).
- [54] N. Joo *et al.*, Eur. Phys. J. B **52**, 337 (2006).
- [55] Eq. (12) in Ref. [37] gives a similar expression for  $\sigma_{zz}$  in the case of multiple tunneling amplitudes  $t_l$ . However, it contains an error and should be replaced by the correct Eqs. (13) and (16) given here.
- [56] In Secs. IV and VI, we ignore the tunneling amplitude  $t'_c$  introduced in Sec. III and consider only the main amplitude  $t_c$ . The effects discussed in Secs. IV and VI can be obtained already at  $t'_c = 0$ .
- [57] J.P. Eisenstein *et al.*, Phys. Rev. B **44** 6511 (1991).
- [58] J.A. Simmons *et al.*, Phys. Rev. B **47** 15741 (1993).
- [59] V.M. Yakovenko and B.K. Cooper, Physica E **34**, 128 (2006).
- [60] G.D. Mahan, *Many-Particle Physics*, 2nd ed. (Plenum Press, New York 1990).
- [61] S. Haddad *et al.*, Phys. Rev. B **72**, 085104 (2005).
- [62] S. Uji *et al.*, Phys. Rev. B **53**, 14399 (1996).
- [63] W. Kang, S.T. Hannahs, and P.M. Chaikin, Phys. Rev. Lett. **70**, 3091 (1993); H. Shinagawa *et al.*, Physica B **201**, 490 (1994); Synth. Met. **70**, 759 (1995);

- E.I. Chashechkina and P.M. Chaikin, Phys. Rev. B **56**, 13658 (1997).
- [64] H. Yoshino *et al.*, J. Phys. Conference Series **51**, 339 (2006); J. Low Temp. Phys. **142**, 323 (2007).
- [65] P.A. Goddard *et al.*, Phys. Rev. B **69**, 174509 (2004).